Experimental and Numerical Analysis of Whistling in Flows around Side-View Mirrors

Arnaud Stoffel, Florent Margnat, Christian Prax, François van Herpe

16ème Congrès Français d'Acoustique
11-15 Avril 2022, Marseille

Experimental and Numerical Analysis of Whistling in Flows around Side-View Mirrors

A. Stoffel[a], F. Margnat[b], C. Prax[b], and F. Van Herpe[a]

[a]Stellantis, Centre Technique de Vélizy,
route de Gisy, Parc Innovel Sud, 78943 Vélizy-Villacoublay, France
[b]Institut Pprime - CNRS, Université de Poitiers et ISAE-ENSMA,
B17 - 6 rue Marcel Doré, TSA 41105, Cedex 9, 86073 Poitiers, France

In the frame of the OpenLab Fluidics@Poitiers, partnership between Institut Pprime and Stellantis, the flow induced whistlings around automotive side-view mirrors are studied by experimental and numerical approaches. Two side-view mirrors that only differ by a step on their caps are analysed at two free stream velocities, 26 and 34 $m.s^{-1}$. A previous experimental campaign using hot-wire anemometer and synchronised microphones is compared to the results of a Time Resolved Particle Image Velocimetry (TR-PIV) and synchronised microphone, both undertaken in the anechoic wind tunnel BETI (Bruit-Environnement-Transport-Ingénierie). Moreover, a Reynolds Averaged Navier-Stokes (RANS) simulation is performed using ANSYS Fluent, for each configuration.
After extracting a maximum of space-time and space-frequency information from the experimental measurements, an exhaustive comparison of the data generated by the three approaches is undertaken in order to evaluate the capacity of the RANS simulation to reproduce the representative elements of the whistlings. Finally, the RANS fields are particularly analysed in the regions responsible for the whistlings, identified during the synchronised hot-wire anemometer - microphones campaign.

1 Introduction

Since the automotive industry is currently facing a drastic technological shift from internal combustion engines (ICE) to quieter electric engines, the contribution of aerodynamic noise to the global interior noise might be enhanced. Therefore, aeroacoustics is more than ever a matter of interest for the passengers' comfort. The flow around side-view mirrors may generate whistlings emerging of a broadband noise. Tonal noise, such as whistling, is particularly perceived as annoying by customers and must therefore be avoided. Nowadays, aerodynamic noise optimization still relies mostly on expensive wind tunnel tests or on prohibitive transient CFD simulations. The aim of this paper is to understand from the experimental measurements the physical phenomenon responsible for the whistling, such as to avoid it at the early design stage. Moreover, the ability of a RANS simulation to reproduce the necessary whistling conditions is investigated.

In the present study, two side-view mirrors (figure 1) that only differ by their caps are studied. The SteppedLine side-view mirror has a step on the top of it in order to create turbulence in the flow that is passing by. This turbulent flow transitioned from laminar to turbulent at the step, upstream the detachment line (design edge, (- - -) in figure 1). In contrary with the BaseLine side-view mirror that may transition from laminar to turbulent flow due to instability when passing the design edge. Desquesnes et al. [2] demonstrated that the creation of vortices just upstream the trailing edge of NACA airfoil is responsible for whistling acoustic radiation. Frank et al. [3] were able to confirm this scenario in the case of an automotive side-view mirror.

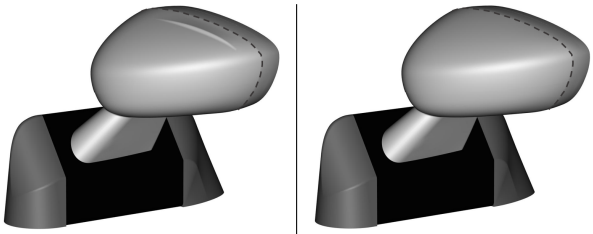

SteppedLine *BaseLine*

FIGURE 1 – SteppedLine and BaseLine side-view mirrors (- - -) : Design edge.

The paper is organised as follows : first, the whistling sources location, located by Lazure et al. [4] using the Hot-Wire Anemometer (HWA) experiment, are confirmed by Time Resolved Particle Image Velocimetry (TR-PIV) experiment. Secondly, a space-time and space-frequency analysis of the TR-PIV data is undertaken. Most of aerodynamic project application being based on RANS simulations, RANS simulations of the interested cases using the 2 different experimental data are validated. Finally, a first analysis of the capacity of the RANS simulation to reproduce the necessary whistling conditions is investigated.

2 Experimental investigation

2.1 Anechoic wind tunnel BETI

The anechoic wind tunnel BETI (Bruit-Environnement-Transport-Ingénierie) is located in the premises of the University of Poitiers on the ENSI-Poitiers site. With an open test-section located in a 90 m^3 plenum acoustically treated, this wind tunnel reproduces free field conditions from 200 Hz. It allows the study and optimization of the flow around obstacles and the associated acoustic radiation. It is depicted in figure 2 and its main characteristics are :

- Test-section area of 0.7×0.7 m^2 and length of 1.5 m
- Rate of turbulence of less than 0.5 %

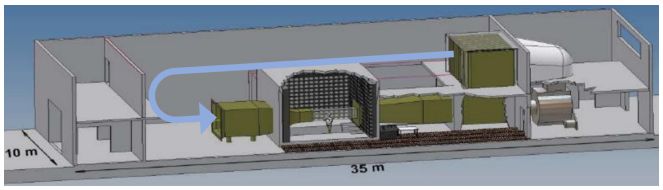

FIGURE 2 – Anechoic wind tunnel BETI.

2.2 Methodology

Two different experimental campaigns were conducted. Synchronised Hot-Wire Anemometer (HWA) and microphones study was undertaken and analysed by Lazure et al. [4]. After testing 0, 5, 10 and 15° yaw angle

with a free stream velocity increasing from 15 to 50 m.s^{-1}, 15° of yaw angle (angle where the mirror plane is orthogonal to the airflow) at 26 and 34 m.s^{-1} were retained to be good conditions for a deeper analysis of the whistling phenomenon. Therefore, 8 HWA profiles were recorded using those conditions, 5 mm downstream the side-view mirrors (figure 3). The acquisition time is of 10 seconds and for hot-wire anemometer as well as acoustic signals, the sampling frequency is of 25.6 kHz. 4 microphones were recording the acoustic radiation during this study but only the relevant Microphones 1 & 2 were presented.

Time Resolved Particle Image Velocimetry (TR-PIV) experiment was conducted in 2016. The side-view mirrors had an yaw angle of 15° and both 26 and 34 m.s^{-1} as free stream velocity (U_0) were studied. 5 planes were recorded for the SteppedLine side-view mirror (figure 3) and the 3 highest of them for the BaseLine side-view mirror ($Z = 19,\ 0$ & -20 mm), by a high-speed camera placed on the top of the side-view mirrors. A synchronized microphone was also recording the acoustic radiation 1 m high above the side-view mirrors (Microphone 1). The TR-PIV planes measurements last 2 seconds with a 20 kHz sampling frequency, that corresponds to 39 999 shots per velocity per side-view mirror. The plane space resolution is about 1 point every 1.3 mm.

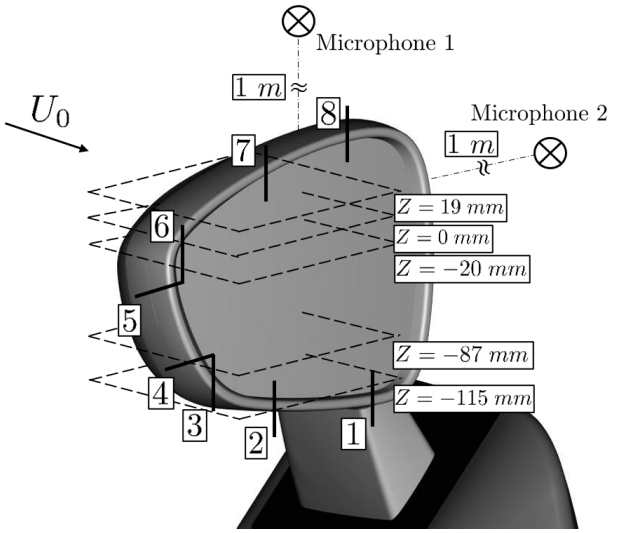

FIGURE 3 – Side-view mirrors nomenclature : HWA profiles, TR-PIV planes, and microphones positions.

2.3 Whistling noise characterisation

During the HWA experiment, 2 Whistlings Frequencies (WF 1 & 2 in table 1) were noticed for each side-view mirror, at each free stream velocity (26 and 34 m.s^{-1}). The TR-PIV experiment reproduced the main whisling (WF 1) at a frequency slightly higher than for the HWA experiment. The second whistling (WF 2) is well emerging for the 26 m.s^{-1} free stream velocity, but stands less out for 34 m.s^{-1}.

From 26 to 34 m.s^{-1}, the BaseLine side-view mirror main whistling frequency increased by more than 500 Hz, but for the SteppedLine side-view mirror by more than the double (+1000 Hz). Both side-view mirrors second whistling frequency increased also of more than 1000 Hz. A third whistling only appeared for the SteppedLine side-view mirror at 26 m.s^{-1}, at a frequency close to the main whistling frequency (approximatly +400 Hz).

The main whistling is emerging in all acoustic measurements, but the other whistlings did not emerge at every recording as clearly, especially in the TR-PIV experiment, except fot the WF 3 of the SteppedLine side-view mirror at 26 m.s^{-1} that emerged especially during the TR-PIV experiment. The intermittence of the phenomenon and the non-intrusive TR-PIV method compared to pertubated HWA experiment flows, but especially the great sensitivity of this phenomenon may explain this variance.

The main whistling frequency is different from one side-view mirror to the other for a given velocity. Nevertheless, the second whistling frequency seems stable from one side-view mirror to the other. The side-view mirrors differing by only the top of them, this implies that the shape of the top of the side-view mirror interfers in the main whistling's phenomenon.

TABLE 1 – Whistlings Frequencies (WF, in Hz) in the acoustic signals.

Line	U_0 (m.s^{-1})	Exp.	WF 1	*WF 2*	*WF 3*
Base	26	HWA	2303	*1430*	-
		PIV	2360	*1460*	-
	34	HWA	2840	*2630*	-
		PIV	2929	-	-
Stepped	26	HWA	2165	*1437*	*2540*
		PIV	2246	*1464*	*2685*
	34	HWA	3171	*2512*	-
		PIV	3295	*(2563)*	-

2.4 Source location

Werner et al. [5] associated tonal noise emission with boundary layer instabilities considering the velocity fluctuation within the shear layer (measured by hotwire). Lazure et al. [4] located the whistling sources by calculating the coherence between the HWA (5 mm downstream the side-view mirror) and the microphone signals. Figure 4.a represents the 3 HWA mean velocity profile (left and top axis), as well as the Power Spectral Density (PSD) of the velocity fluctuation in function of the distance along the HWA profile line (left and bottom axis) for the SteppedLine side-view mirror at 26 m.s^{-1}. When the distance is close to the trailing edge of the side-view mirror, where the velocity gradient is the highest, a peak at the same frequency as the acoustic whistling is emerging in the velocity fluctuation PSD (figure 4.b). Expanding this postprocessing to all HWA data, a source location confirmed Lazure et. al [4] conclusions, as presented in figure 5.

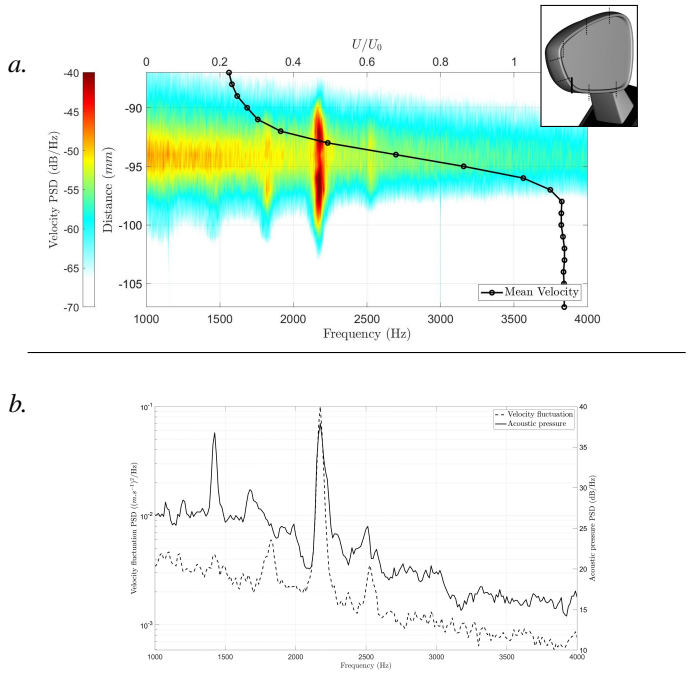

FIGURE 4 – SteppedLine side-view mirror 3 HWA profile at 26 m.s^{-1} : Mean velocity profile & velocity fluctuation PSD in function of the distance along the HWA profile line (*a*), -96mm HWA point PSD compared to synchronous microphone 1 acoustic PSD (*b*).

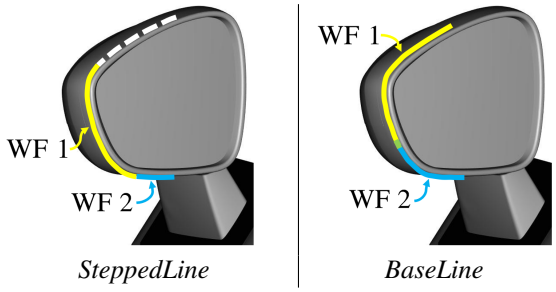

FIGURE 5 – SteppedLine and BaseLine side-view mirrors sources locations.

The yellow line (—) corresponds to the main whistling (WF 1) while the blue line (—) corresponds to the second whistling (WF 2). The dotted white line on the SteppedLine side-view mirror represents the region where the whistling is attenuated thanks to the step on the cap of this side-view mirror. Nevertheless, this step seems to reinforce the whistling on the side of the side-view mirror.

The TR-PIV planes are here analysed in the frequency domain, using the PSD of each point in space, in order to confirm the whistling source location. The TR-PIV Z=-20 mm plane of the SteppedLine side-view mirror at 26 m.s^{-1} is presented in figure 6.a at a frequency of 2246 Hz (WF 1), in figure 6.c at a frequency of 2715 Hz (WF 3) and in figure 6.b at a frequency in between, where no whistling is emerging. Acoustic and velocity fluctuation (at an energetic point downsteam the trailing edge, *(P)* in figure 6.a) PSD are compared in the figure 6.d. As for HWA, peaks at the same frequency as the acoustic whistlings is emerging in the velocity fluctuation PSD. The 3 TR-PIV top planes of the BaseLine side-view mirror confirmed the source location. The 5 TR-PIV planes of the SteppedLine side-view mirror confirmed the source location except for the bottom part of the side-view mirror where a peak at the main whistling frequency is found in the frequency spectrum of the velocity downstream the trailing edge. The Z=0 mm plane velocity spectrum has an emerging peak only for the BaseLine side-view mirror, confirming that the step on the cap of the SteppedLine side-view mirror reduces/cancels the whistling in this upper region. The most energetic flow is located around the side-view mirror, in the boundary layer and lighter downstream the trailing edge. The tubulent energy seems to fall when passing the trailing edge, except at the whistlings frequency where the energy is maintained for a small distance after the trailing edge.

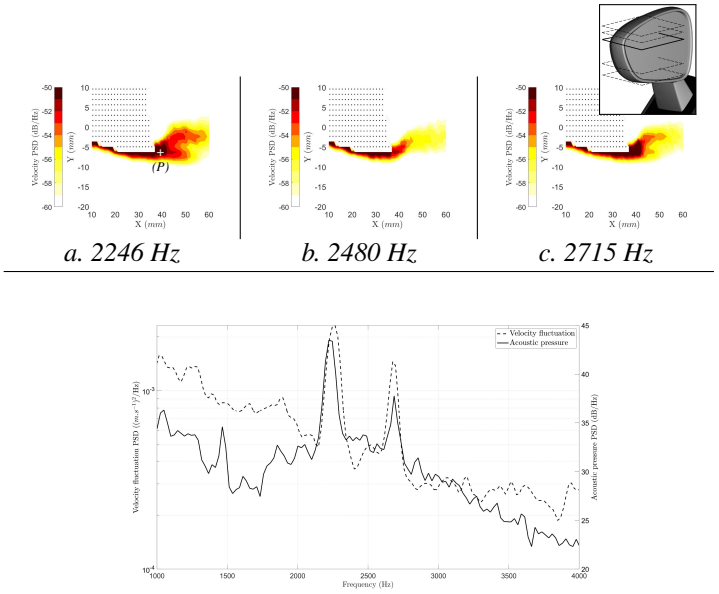

a. 2246 Hz *b. 2480 Hz* *c. 2715 Hz*

d. Downstream trailing edge (P) TR-PIV point PSD compared to synchronous acoustic PSD

FIGURE 6 – SteppedLine side-view mirror Z=-20 mm TR-PIV plane at 26 m.s^{-1} : Frequency domain.

2.5 Space-time & space-frequency energy

2D velocity vectors are calculated by the TR-PIV measurements (along x- and y-direction). Therefore, different scalars have been postprocessed from this data, such as averaged velocity magnitude, Root Mean Square (RMS) velocity fluctuation (noted U'_{RMS} in equation 1), or averaged vorticity (figure 7).

$$U'_{RMS} = \sqrt{((U_x - \overline{U_x})_{RMS})^2 + ((U_y - \overline{U_y})_{RMS})^2} \quad (1)$$

An acceleration zone is noticed at the design edge of the side-view mirror, where detachment occurs. RMS velocity fluctuations reach the biggest values in the shear layer, as well as further downstream the trailing edge. The RMS velocity fluctuation having big values in the shear layer means that the shear layer is fluctuating through time and therefore may be unstable. Vorticity is important in the boundary layer and is then decreasing downstream the trailing edge. The mean vorticity magnitude in space is close to the energy repartition in the frequency domain, vorticity being the main source of turbulent energy. Nevertheless, the TR-PIV resolution is causing the velocity near wall field to go from 0 m.s^{-1} to the acceleration zone, making a fine analysis of the shear layer impossible.

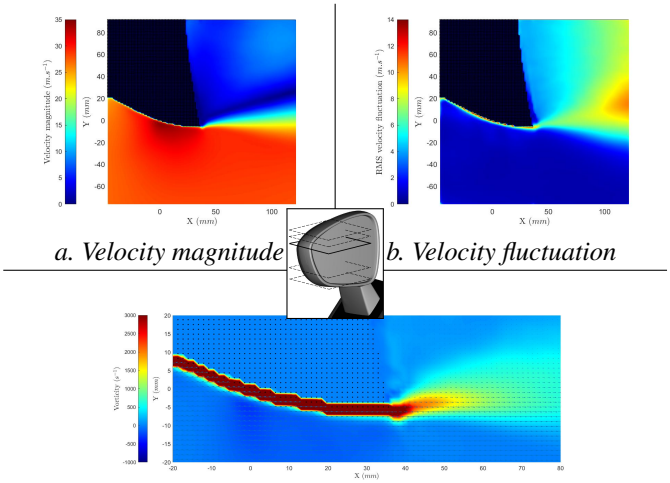

FIGURE 7 – Velocity magnitude (*a*), Velocity fluctuation RMS (*b*), and Vorticity (*c*) of Z=-20 mm TR-PIV plane for SteppedLine side-view mirror at 26 m.s^{-1}.

The vorticity at a given time step is shown figure 8. Downstream the trailing edge (dotted white line), and along the solid white line *(S)*, the vortices structure is clearly noticeable. Therefore, along the *(S)* line, the transverse velocity fluctuation (y-direction) is represented versus time. Upstream the trailing edge, the velocity fluctuation exhibits horizontal spots. This shape can be explained by the sudden apparition and disparition of energy at those measured points, physically meaning a transverse oscillation of the flow at this location. Nevertheless, knowing that the shear layer thickness is lower than the resolution of the TR-PIV, the lack of resolution in this region may unable a clear conclusion. Downstream the trailing edge, the convection of the transverse velocity fluctuation, and therefore the vortices, is clearly put forward. In the case of the SteppedLine side-view mirror represented in this figure, vortices are created periodically by small group of 3. Therefore, an alternance in the creation of vortices and a flow at rest is occuring.

Using the same methodology for each side-view mirror at each velocity, the transverse velocity fluctuation PSD along the *(S)* line is presented figure 9.

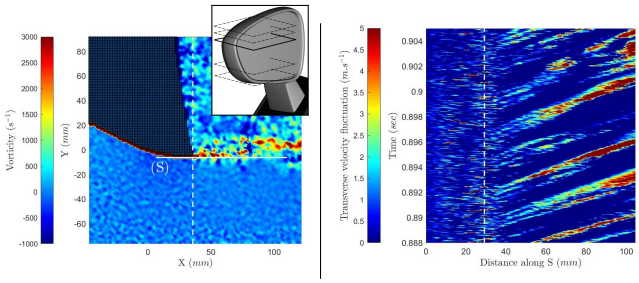

FIGURE 8 – SteppedLine side-view mirror Z=-20 mm TR-PIV plane at 26 m.s^{-1} : instantaneous vorticity field (left), time-space map of the transverse velocity fluctuation along the *(S)* line (right).

For the SteppedLine side-view mirror, a peak at the acoustic whistling frequency emerges, corresponding in the time domain at the time scale between 2 vortices in a group of 3 ($\approx$ 0.0004 seconds). Moreover, several peaks separated from around 400 Hz are emerging in the frequency spectrum, corresponding in the time domain at the time scale between 2 group of vortices. The same 400 Hz is found in the Hot-Wire Anemometer velocity PSD (figure 4). In this particular case of the SteppedLine side-view mirror at 26 m.s^{-1}, 2 acoustic whistlings emerged (WF 1 & WF 3) separated from 400 Hz. It is possible that the oscillation of the flow at 400 Hz is exciting whistlings 400 Hz from the main whistling. For the BaseLine side-view mirror, a peak at the acoustic whistling frequency emerges in the frequency spectrum without other maximums as emerging as for the SteppedLine side-view mirror. The step on the SteppedLine side-view mirror cap may therefore interfer in this oscillating phenomenon. The emerging frequencies in this figure are consistent with the whistling source location.

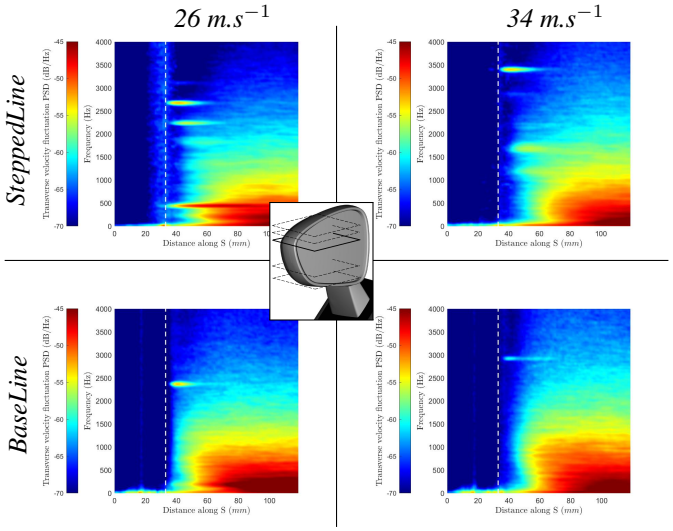

FIGURE 9 – Transverse velocity fluctuation PSD along *(S)* line in Z=-20 mm TR-PIV plane.

3 RANS simulations

For the whistlings deeper understanding, near wall flow is the most important since the source of the phenomenon takes it place. TR-PIV planes resolution is too coarse in order to have points in the boundary layer, and HWA profiles are about 5 mm downstream the trailing edge. Numerical simulations are therefore needed in order to have new informations in the whistlings sources regions. RANS simulations are the most common CFD simulations used in the automotive's applications and are easily accessible (very low CPU time consumption). Therefore, extracting a maximum of informations from the RANS model is important in order to avoid going into costly experiment or direct noise computation blindly or unnecessarily.

3.1 Methodology

The RANS simulations were computed using ANSYS Fluent's $k-\epsilon$ realizable model [1]. The convergence of the solution presented here has been tested by looking at the results at each RANS iteration for a mesh size doubled and halved. The validated simulation is running in 7 min 17 sec in Stellantis Cluster (compared to 3 min 52 sec and 26 min 58 sec respectively for a mesh doubled and halved) with a mesh composed of a total of 15 prism layers with the first prism height of 0.020 mm and a growth rate of 1.34, a refined box around the side-view mirror with a mesh size of 3.125 mm, and the far field meshed at a mesh size of 50 mm.

3.2 RANS validation

First, the computed velocity magnitude using only the x- and y-velocity components are compared to the TR-PIV averaged planes (figure 10). The flow around the side-view mirror is well reproduced, even if differences are noticed in the wake. Planes are comparable as 2D colored planes, and for a more accurate comparison, the velocity along a line (downstream the trailing edge) for experimental and numerical results are plotted in figure 10.c.

Secondly, HWA mean profiles are compared to the RANS simulations for both side-view mirrors in figure 11. The profile in the figure 11.a is the one downstream the step of the SteppedLine side-view mirror. Therefore, a net disctinction between the 2 side-view mirrors is visible for the HWA data. The RANS was able to differentiate the 2 side-view mirrors as well even if the differences are smaller. The profile in the figure 11.b, located on the bottom of the side-view mirrors, is less impacted by the step and experimental and numerical results are closer one to another. HWA is not able to measure velocity under 5 m.s^{-1}, making the low velocity region from experiment unknown. Moreover, a slight uncertainty between the RANS and the HWA profile coordinates is to take into account in this comparisons. In both profile, the RANS is slightly overestimeting the acceleration zone.

Concerning both experimental comparisons, RANS simulations are computing the steady-state flow which may explain the differences to averaged flow.

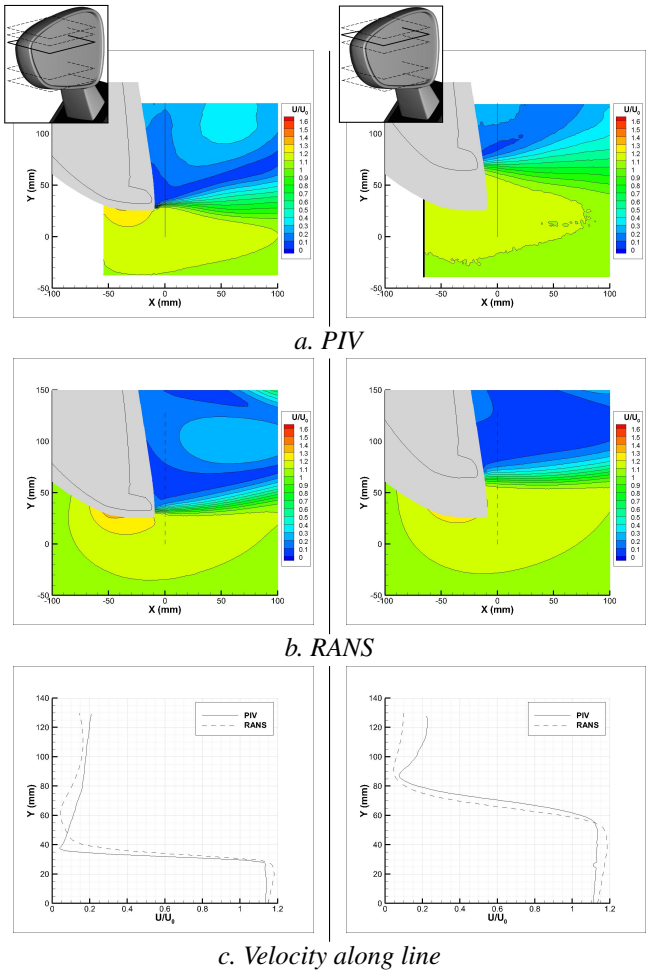

FIGURE 10 – PIV and RANS Z=-20 mm (left) and Z=0 mm (right) planes comparison for BaseLine side-view mirror at 26 m.s^{-1}.

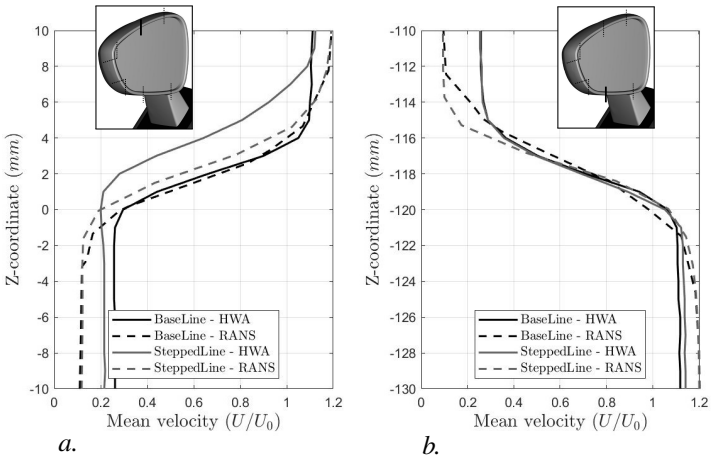

FIGURE 11 – [7] (*a*) & [2] (*b*) HWA profiles compared to RANS results for both side-view mirrors at 26 m.s^{-1}.

The pressure coefficient at the surface of the side-view mirrors ($\frac{p-p_0}{(1/2)\rho_0 U_0^2}$), plotted in figure 12, put forward that the RANS simulations were also able to reproduce the detachment of the flow at the design edge, as well as at the step for the SteppedLine side-view mirror.

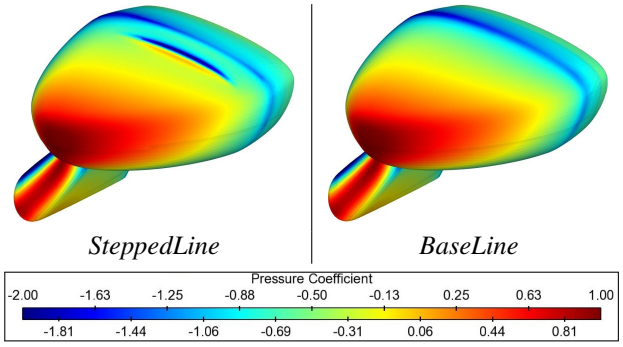

FIGURE 12 – Wall pressure coefficient for $U_0 = 34$ m.s^{-1}.

3.3 RANS extraction

Entire field mean flow is given by the RANS simulation. The pressure coefficient around the trailing edge of the side-view mirrors for all cases is presented figure 13. The pressure coefficient for all cases are very close one to another up to 130 mm (inner face). Further away on the trailing edge (220 mm), the step of the SteppedLine side-view mirror modifies the pressure coefficient. The effect of the step is not only visible on the top, but on the outer side (310 - 420 mm), as well as on the bottom (420 - 480+ mm) of the side-view mirrors, where no geometrical difference exists. The presence of the step changes the flow not only on the top of the side-view mirror but around half the side-view mirror, at locations corresponding to the whistlings sources regions. For the outer and lower side, the normalization by the dynamic head of the pressure is not sufficient to cancel the influence of the free stream velocity on the pressure field.

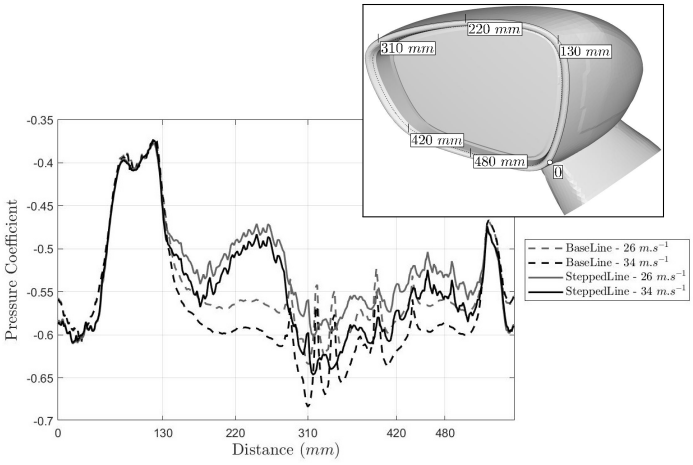

FIGURE 13 – Pressure coefficient along the trailing edge.

Furthermore, the step of the SteppedLine side-view mirror generates vorticity along the Z-direction near the outer side of the side-view mirror (figure 14). The whistling on this side of the side-view mirror is linked to vortices in this direction. Therefore, those new vortices may reinforce the whistling on the side of the side-view mirror.

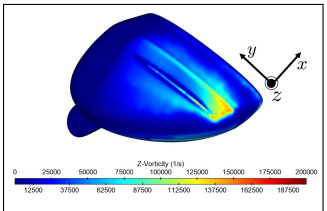

FIGURE 14 – Z-vorticity at the surface for the SteppedLine side-view mirror.

4 Conclusion & prospects

Two whistling side-view mirror geometries only differing by their caps are studied at two free stream velocity. The TR-PIV measurements confirmed the whistling frequencies and the sources location around the side-view mirror concluded from the HWA experiment. Spatial analysis from the TR-PIV planes enabled a better understanding of the flow induced whistlings generation phenomenon. The time-scale between 2 vortices corresponds to the tonal noise period, and the creation of vortices is periodically interrupted by a low frequency oscillation for the SteppedLine side-view mirror. Finally, a RANS simulation of each case is validated by experimental data as steady-state flow. Moreover, whistling representative informations such as the detachment location, as well as differences between the 2 side-view mirrors are noticed around half the side-view mirrors, at locations corresponding to the whistlings sources regions.

One perspective for this work is to study the stability of the RANS steady-state flow in order to stimulate the unstable flow, responsible for the whistlings, and identify indicators making a prediction in terms of whistlings possible.

References

[1] ANSYS, Inc. *FLUENT Theory Guide, 4.3.3 Realizable $k-\epsilon$ Model*.

[2] G Desquesnes, M Terracol, and P Sagaut. Numerical investigation of the tone noise mechanism over laminar airfoils. *Journal of Fluid Mechanics*, 591 :155–182, 2007.

[3] Hannes M Frank and Claus-Dieter Munz. Direct aeroacoustic simulation of acoustic feedback phenomena on a side-view mirror. *Journal of Sound and Vibration*, 371 :132–149, 2016.

[4] H. Lazure, V. Morinière, J. Laumonier, and L. Philippon. Sifflement aérodynamique d'un rétroviseur. In *Actes du 13e Congrès Français d'Acoustique joint avec le colloque VIbrations, SHocks and NOise*, pages 1891–1897, 2016.

[5] MJ Werner, W Würz, and E Krämer. Experimental investigation of an aeroacoustic feedback mechanism on a two-dimensional side mirror model. *Journal of Sound and Vibration*, 387 :79–95, 2017.